A Calculation of the Neutron (111,$\bar{1}\bar{1}$1/220) Three Beam Case *

W. Treimer

Fritz-Haber-Institut der Max-Planck-Gesellschaft, Berlin-Dahlem

Z. Naturforsch. **37a**, 490–500 (1982); received February 23, 1982

Dedicated to Professor G. Hildebrandt on the occasion of his 60th Birthday

After the development of a very common formalism for neutron three beam cases, a detailed investigation is given for the case (111, $\bar{1}\bar{1}$1/220) and a comparisation with the (different) case (111, $\bar{1}$11/200) is presented. It is shown that the former case behaves different by concerning dispersion branches and reflection curves; both are asymmetric in respect to a wave incident in the exact Bragg direction and react more sensitive by upon small deviations of the incident wave from this direction. Simple formulae were found for the reflection curves of the intensities for all three beams behind a perfect crystal slab and the Pendellösung period.

1. Introduction

If a beam of (X-ray or neutron) waves with wavevectors $\boldsymbol{k}_i$ enters a crystal in such a way that the Bragg equation is satisfied simultaneously for two different sets G and H of netplanes, then the conditions of a three beam case (TBC) are given and three waves with wavevectors $\boldsymbol{k}_0$, $\boldsymbol{k}_G$, $\boldsymbol{k}_H$ are excited in the crystal which are combined with each other by $\boldsymbol{k}_G = \boldsymbol{G} + \boldsymbol{k}_0$ and $\boldsymbol{k}_H = \boldsymbol{H} + \boldsymbol{k}_0$ ($\boldsymbol{G}$, $\boldsymbol{H}$ reciprocal lattice vectors).

Particular effects in many beam cases with X-rays have been known since long. In 1935 Renninger detected the effect of "Umweganregung" [1]: a "forbidden" reflection gets intensity via the detour about two "allowed" reflections which are excited simultaneously.

Thirty years later Borrmann and Hartwig detected another effect strictly bound to the perfect lattice, the so-called "enhanced Borrmann effect", when they examined wide angle diagrams of a Ge crystal plate [2]: they found enhanced intensities at the intersections of the Kossel lines of certain reflections. The absorption, already decreased due to the Borrmann effect of the two beam case, must have been reduced considerably more. The most pronounced effect was observed in the case of simultaneous diffraction on (111) and ($\bar{1}$11). Borrmann and Hartwig proposed to understand the enhanced decrease of absorption as resulting from a more favourable adaptation of the wave fields of this TBC to the lattice. Shortly later G. Hildebrandt confirmed this assumption by calculating the accomodation and the minimum coefficients of this particular case [3], [4], which in the following will be denoted as (111, $\bar{1}$11/200) ((200) is the "coupling" netplane).

Some of the following work treated the seemingly similar TBC (111, $\bar{1}\bar{1}$1/220) which, however, was found to behave quite different by [5], [6], [7].

In the following we restrict our considerations to these two TBC's, which have been discussed (for X-rays) in some detail in [5]. In X-ray TBC's the dispersion surface consists of six sheets ($2n$ sheets in an n beam case, Ewald 1917); in thick perfect crystals, however, only the sheets closest to the Laue point need be considered, because only wavefields from these sheets undergo restricted absorption (Ewald [8]).

In the case of neutron diffraction the calculations are simplified due to the absence of absorption**; the dispersion surface of a TBC then consists of only three sheets. On the other hand, due to negligibly small absorption, all possible (excited) wavefields are present within the lattice and have to be taken into account throughout the calculations; their

* This work was partially supported by the BMFT, project Nr. 03-41 E 06 P.

Reprint requests to Dr. W. Treimer, Fritz-Haber-Institut d. Max-Planck-Gesellschaft, 1000 Berlin-Dahlem.

** There are, however, measurements with thicker absorbing crystals (calcite and cadmium sulfate crystals) using (n, γ) processes to determine the imaginary parts of the excitation errors [9], as well as investigations with indium antimonide crystals [10], [11] and thick ideal perfect crystals dealing with anomalous absorption of neutrons in matter [12].

0340-4811 / 82 / 0500-0490 $ 01.30/0. — Please order a reprint rather than making your own copy.

interferences in the lattice of (some mm) thick crystals give rise to the observation of pendellösung effects (e.g. [13]).

In previous papers [14], [15] detailed calculations were given for the (111, $\bar{1}$11/200) neutron three beam case (NTBC). The now presented general formulation of the (111, $\bar{1}\bar{1}$1/220) NTBC shall enable us to study dispersion surfaces, amplitudes of excited waves, Pendellösung intensities etc. and to compare the results to those of the (111, $\bar{1}$11/200) NTBC. The calculations were done for silicon, absorption has been neglected totally.

As already stated, one of the main differences between X-ray TBC's and NTBC's lies in the fact that one expects to get Pendellösung effects in the latter cases. It will be shown in particular that the Pendellösung period

$$\Delta_0 = \pi \cos\theta / N \lambda F_{hkl}$$

(θ_B Bragg angle, N number of unit cells, $F_{hkl} = F b_c e^{-W}$, F structure factor, b_c coherent scattering amplitude, W Debye-Waller factor) for the usual two beam case is strongly related to the formula of the pendellösung period of the three beam case. All calculations were done for the diamond lattice, which has an inversion center so that the Fourier components for the interaction potentials are $V(\boldsymbol{G}) = V(-\boldsymbol{G})$. The calculation itself is split into two parts, a symmetrical and an asymmetrical one. The symmetrical calculation assumes the incoming wave vector $\boldsymbol{k}^i$ to remain within the plane of symmetry, the plane symmetrical to the reflecting (111) and ($\bar{1}\bar{1}$1) netplanes, i.e. (220) in this case. In the asymmetric calculations we allow the incoming wave vector $\boldsymbol{k}^i$ to leave the (220) plane. Dispersion surfaces, ψ-functions and reflection curves were calculated always in the same angular range of incidence 6.4″.

2. Fundamental Equations

The interaction of a neutron wave with matter is described by the Schrödinger equation

$$H\psi = E\psi, \tag{1}$$

where H means the Hamilton operator and E the total energy of the system:

$$H = -\frac{\hbar^2}{2m}\nabla^2 + V(\boldsymbol{r}), \quad E = \frac{\hbar^2 k^2}{2m}. \tag{1a}$$

$V(\boldsymbol{r})$ is the interaction potential, also called the Fermi pseudo potential, and has for pure coherent nuclear interaction the form [16]

$$V(\boldsymbol{r}) = \frac{2\pi\hbar^2 b_c}{m} \sum_j \delta(\boldsymbol{r} - \boldsymbol{r}_j) \tag{2}$$

($\boldsymbol{r}$ is the position vector, $\boldsymbol{r}_j$ the vector pointing at the lattice position, b_c means the coherent scattering amplitude for $\boldsymbol{r}_j = \boldsymbol{0}$). The δ-shape guarantees isotropic scattering at the Born approximation [17].

We assume the ψ function to be a Bloch wave with the amplitude $u(\boldsymbol{r})$ and with the periodicity of the lattice,

$$\begin{aligned} \psi(\boldsymbol{r}) &= u(\boldsymbol{r}) \exp\{i\boldsymbol{K}_0 \cdot \boldsymbol{r}\}, \\ u(\boldsymbol{r}) &= \sum_G u(\boldsymbol{G}) \exp\{i\boldsymbol{G} \cdot \boldsymbol{r}\}, \end{aligned} \tag{2a}$$

and get as the solution of the Schrödinger equation the fundamental equation of dynamical neutron scattering

$$\begin{aligned} &[\hbar^2/2m \,|\, \boldsymbol{K}_0 + \boldsymbol{G}|^2 - E]\, u(\boldsymbol{G}) \\ &= -\sum_{G'} V(\boldsymbol{G} - \boldsymbol{G}')\, u(\boldsymbol{G}). \end{aligned} \tag{3}$$

$\boldsymbol{K}_0$ is the incident wave vector in the crystal, already corrected for the refraction of $\boldsymbol{k}^i$ (vacuum wave vector) at the boundaries of the crystal. G, G' are reciprocal lattice points, $V(\boldsymbol{G} - \boldsymbol{G}')$ is the Fourier transform of the interaction potential $V(\boldsymbol{r})$. If only the origin of the reciprocal lattice is hit by the Ewald sphere, i.e. if $\boldsymbol{G} = \boldsymbol{G}' = \boldsymbol{0}$, one gets as the solution of (3) the index of refraction

$$n = \frac{K_0}{k_i} = 1 - \frac{1}{2}\frac{V(\boldsymbol{0})}{E} = 1 - \frac{\lambda^2 b_c N}{2\pi}.$$

With two points lying on or close to the Ewald sphere one has the well known two beam case, and if three reciprocal points come into play a three beam case is realized. $\boldsymbol{G}'$ principally is directed to all points of the reciprocal lattice but only those are considered in the calculation which strongly come into play, namely those which are situated at or very close to the Ewald sphere [18], [19].

The system of equations (3) has to be solved to determine ε_0, ε_G and ε_H, the individual Anregungsfehler (excitation errors):

$$\begin{aligned} (2\varepsilon_0 + V_0)\, u_0 + V_{-G}\, u_G + V_{-H}\, u_H &= 0, \\ V_G\, u_0 + (2\varepsilon_G + V_0) + V_{G-H}\, u_H &= 0, \\ V_H\, u_0 + V_{H-G}\, u_G + (2\varepsilon_H + V_0)\, u_H &= 0, \end{aligned} \tag{4}$$

where ε_0, ε_G and ε_H are defined by

$$\frac{|\boldsymbol{K}_0|^2 - \boldsymbol{k}^{i2}}{\boldsymbol{k}^i} = 2\varepsilon_0; \quad \frac{|\boldsymbol{K}_0 + \boldsymbol{G}|^2 - \boldsymbol{k}^{i2}}{\boldsymbol{k}^{i2}} = 2\varepsilon_G; \quad \frac{|\boldsymbol{K}_0 + \boldsymbol{H}|^2 - \boldsymbol{k}^{i2}}{\boldsymbol{k}^{i2}} = 2\varepsilon_H \tag{5}$$

(with the abbrevations

$$V_{M+N} = \frac{V(\boldsymbol{M} + \boldsymbol{N})}{E}, \quad M, N = 0, G, H;$$
$$u(0) = u_0, \quad u(G) = u_G, \quad u(H) = u_H$$

are the amplitudes for the 0, G and H directions). Later on we will add to the excitation error ε the indices 1, 2 or 3 to denote the individual dispersion branches. The Fourier component $V(\boldsymbol{M} \pm \boldsymbol{N})$ has primary influence on the type of the three beam case. We consider a diamond lattice, where the Fourier components $V_{G-H} = V(200)$ and $V_{H-G} = V(\bar{2}00)$ are identical by zero (forbidden reflections) in the (111, $\bar{1}$11/200) TBC, but related to strong reflections $V(220)$ and $V(\bar{2}\bar{2}0)$ in the other TBC (111, $\bar{1}\bar{1}$1/220). Especially in the case of neutrons we can set $V(220) = V(0)$. The different cooperation of the third netplane (200) or (220) characterizes the TBC's and determines the shape of the dispersion surfaces and the reflection curves. From (4) one gets a nontrivial solution if and only if the corresponding determinant vanishes, i.e.

$$\begin{vmatrix} 2\varepsilon_0 + V_0 & V_{-G} & V_{-H} \\ V_G & 2\varepsilon_G + V_0 & V_{G-H} \\ V_H & V_{H-G} & 2\varepsilon_H + V_0 \end{vmatrix} = 0. \tag{6}$$

The excitation errors ε_G and ε_H are correlated to ε_0 by the equations

$$2\varepsilon_G = 2\varepsilon_0 \cdot \frac{1}{b_G} + \alpha_G,$$
$$2\varepsilon_H = 2\varepsilon_0 \cdot \frac{1}{b_H} + \alpha_H, \tag{7}$$

where α_G and α_H are defined by

$$\alpha_G = \frac{1}{k^{i2}}[\boldsymbol{G}^2 + \boldsymbol{k}^i \cdot \boldsymbol{G}],$$
$$\alpha_H = \frac{1}{k^{i2}}[\boldsymbol{H}^2 + \boldsymbol{k}^i \cdot \boldsymbol{H}], \tag{8}$$

determining the position of the incident wave vector $\boldsymbol{k}^i$ with respect to the crystal surface and the netplanes. b_G and b_H and the angle γ_0 (angle between $\boldsymbol{k}^i$ and surface normal $\boldsymbol{n}$) are correlated to each other by the equations

$$\frac{1}{b_G} = 1 + \frac{1}{k^i \cos\gamma_0}\boldsymbol{n} \cdot \boldsymbol{G}, \tag{9a}$$
$$\frac{1}{b_H} = 1 + \frac{1}{k^i \cos\gamma_0}\boldsymbol{n} \cdot \boldsymbol{H}$$

with

$$\cos\gamma_0 = \frac{\boldsymbol{k}^i \cdot \boldsymbol{n}}{|\boldsymbol{k}^i| \cdot |\boldsymbol{n}|}. \tag{9b}$$

α_G and α_H contain the Bragg condition; both become zero if $\boldsymbol{k}^i$ is incident at the exact Bragg angle. The basis used for these calculations is an orthogonal coordinate system, built up by the vectors [110], [001] and [1$\bar{1}$0] so $\boldsymbol{n}$ is parallel to [$\bar{1}$10].

The equation corresponding to (6) is of the third degree and its roots are the excitation errors $\varepsilon_{0,1}$; $\varepsilon_{0,2}$; $\varepsilon_{0,3}$ where the numbers 1, 2 and 3 denote the particular sheets.

We further introduce the abbreviations

$$a_G = \frac{1}{k^{i2}}[\boldsymbol{G}^2 + \boldsymbol{k}^i \cdot \boldsymbol{G}] + V_0, \tag{9c}$$
$$a_H = \frac{1}{k^{i2}}[\boldsymbol{H}^2 + \boldsymbol{k}^i \cdot \boldsymbol{H}] + V_0,$$

and insert the relations (7), (8) and (9) into (6). Then we get

$$\begin{aligned} &\varepsilon_0^3 + \tfrac{1}{2}\varepsilon_0^2(a_G b_G + a_H b_H + V_0) \\ &+ \tfrac{1}{4}\varepsilon_0[a_G b_G a_H b_H + V_0(a_G b_G + a_H b_H) \\ &- b_G b_H V_{G-H} V_{H-G} - b_G V_G V_{-G} \\ &- b_H V_H V_{-H}] + \tfrac{1}{8} b_G b_H [V_0(a_G a_H \\ &- V_{G-H} V_{H-G}) + V_G V_{-H} V_{H-G} \\ &+ V_{-G} V_H V_{G-H} \\ &- (a_H V_G V_H + a_G V_H V_{-H})] = 0 \end{aligned} \tag{10}$$

This cubic equation represents the general formulation of a three beam dispersion surface. We will discuss it by means of a particular example, (the symmetrical case) and two common examples (asymmetrical cases).

3. Symmetrical Incidence

In order to distinguish between cases of symmetrical and asymmetrical incidence we introduce an angle α denoting the angle between $\boldsymbol{k}^i$ and the plane of symmetry (220). We start with the sym-

metrical treatment where $\alpha = 0$, and at first we even further simply by assuming the Bragg condition to be exactly fulfid for the (111) and ($\bar{1}\bar{1}$1) netplanes; then in (10) the relations $b_G = b_H = 1$ hold for $\theta = \theta_B$ and (10) becomes a very simple cubic equation with the solutions

$$\varepsilon_{0,1} = 0.0; \quad \varepsilon_{0,2} = V_0 \left[\frac{3}{4} + \frac{\sqrt{5}}{4}\right] \quad \text{and}$$

$$\varepsilon_{0,3} = V_0 \left[\frac{3}{4} - \frac{\sqrt{5}}{4}\right].$$

If we insert these values in the amplitude ratios we find from (4)

$$\frac{u_G}{u_0} = X_j = \frac{V_G V_{-H} - E_{0,j} V_{G-H}}{V_{-G} V_{G-H} - E_{G,j} V_{-H}},$$

$$\frac{u_H}{u_0} = Y_j = \frac{E_{G,j} V_H - V_G V_{H-G}}{V_{H-G} V_{G-H} - E_{G,j} E_{H,j}},$$

$$\frac{u_G}{u_H} = Z_j = \frac{E_{0,j} E_{H,j} - V_{-H} V_H}{V_H V_{-G} - E_{0,j} V_{H-G}}, \qquad (11)$$

where $E_{0,j}$, $E_{G,j}$ and $E_{H,j}$ are expressed by

$$E_{0,j} = 2\varepsilon_{0,j} + V_0,$$
$$E_{G,j} = 2\varepsilon_{G,j} + V_0,$$
$$E_{H,j} = 2\varepsilon_{H,j} + V_0. \qquad (12)$$

Now we are able to determine the amplitude ratios X_j and Y_j. In order to calculate the strength of the particular amplitudes in the crystal we evaluate the intensities and get the following relations for wavefields I, II and III:

Wavefield I

$$|u_{0,1}|^2 : |u_{G,1}|^2 : |u_{H,1}|^2 = 0 : 1 : 1,$$

wavefield II

$$|u_{0,2}|^2 : |u_{G,2}|^2 : |u_{H,2}|^2 = 1 : 0.191 : 0.191,$$

wavefield III

$$|u_{0,3}|^2 : |u_{G,3}|^2 : |u_{H,3}|^2 = 1 : 1.309 : 1.309.$$

The relation for wavefield I is identical with the results of the equivalent X-ray case, where the ratios are given by $I_0 : I_L : I_M = 0 : 1 : 1$ [6]. These intensities are valid for the wavefield penetrating the crystal with minimum absorption at the exact three waves point. All other wavefields suffer higher absorption by passing through the crystal (and only partly reach the exit surface). In the case of neutron diffraction all three wavefields will traverse the crystal coherently with nearly zero absorption and must be taken into account.

Now we allow $\boldsymbol{k}^i$ to move within the (220) plane within the angular range of $\pm 6.4''$. For each position, starting from $-2.2''$, the excitation errors are calculated and plotted as seen in Figure 1a. To calculate the intensities behind a perfect crystal slab we consider the wave function

$$\psi_j(\boldsymbol{r}) = \sum_{G'} \exp\left\{i\left[\frac{\boldsymbol{k}^i \varepsilon_{0,j}}{\cos\gamma_0}\boldsymbol{n} + \boldsymbol{k}^i + \boldsymbol{G}'\right]\cdot \boldsymbol{r}\right\}$$

from (2a), which consists of parts originating from partial waves in the 0, G and H direction. All parts together represent a wavefield, i.e. a linear and independent solution of the Schrödinger Equation (1). To calculate the intensities of the waves in the 0, G and H directions we therefore combine for each direction 0, G, H the (coherent) part of branch 1, 2 and 3, building up wavefields by ψ-functions of different branches. These wavefields can be written as

$$\psi_0(\boldsymbol{r}) = \sum_j \exp\left\{i\left(\frac{k^i \varepsilon_{0,j}}{\cos\gamma_0}\boldsymbol{n} + \boldsymbol{k}^i\right)\boldsymbol{r}\right\} u_j(\boldsymbol{0}), \qquad (13)$$

$$\psi_G(\boldsymbol{r}) = \sum_j \exp\left\{i\left(\frac{k^i \varepsilon_{0,j}}{\cos\gamma_0}\boldsymbol{n} + \boldsymbol{G} + \boldsymbol{k}^i\right)\boldsymbol{r}\right\} u_j(\boldsymbol{G}),$$

$$\psi_H(\boldsymbol{r}) = \sum_j \exp\left\{i\left(\frac{k^i \varepsilon_{0,j}}{\cos\gamma_0}\boldsymbol{n} + \boldsymbol{H} + \boldsymbol{k}^i\right)\boldsymbol{r}\right\} u_j(\boldsymbol{H}).$$

Now these wave functions have to be adapted to the boundary conditions at the surface which are $\boldsymbol{n}\cdot\boldsymbol{r} = 0$, $\psi_0(D) = \psi_e$ ($\psi_e = u \exp\{i\boldsymbol{k}^i \cdot \boldsymbol{r}\}$ is the incoming wave) and $\psi_G = \psi_H = 0$, because no diffracted waves are present. Therefore we get the following inhomogeneous system of equations

$$\sum_j u_j(\boldsymbol{0}) = u, \quad \sum X_j u_j(\boldsymbol{0}) = 0, \quad \sum_j Y_j u_j(\boldsymbol{0}) = 0$$
$$(j = 1, 2, 3) \qquad (14)$$

knowing that in the symmetrical case

$$\sum_j X_j u_j(0) = \sum_j Y_j u_j(0)$$

are linearly dependent. X_j and Y_j are defined by (9) and we easily get the amplitudes

$$u_1(\boldsymbol{0}) = 0, \quad u_2(\boldsymbol{0}) = \frac{X_3}{X_3 - X_2} u,$$

$$u_3(\boldsymbol{0}) = \frac{-X_2}{X_3 - X_2} u. \qquad (15)$$

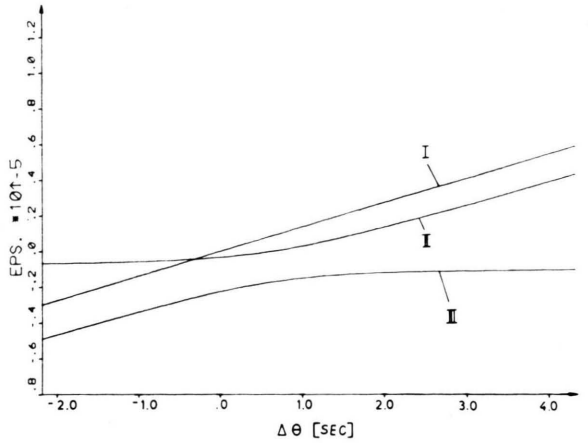

(a)

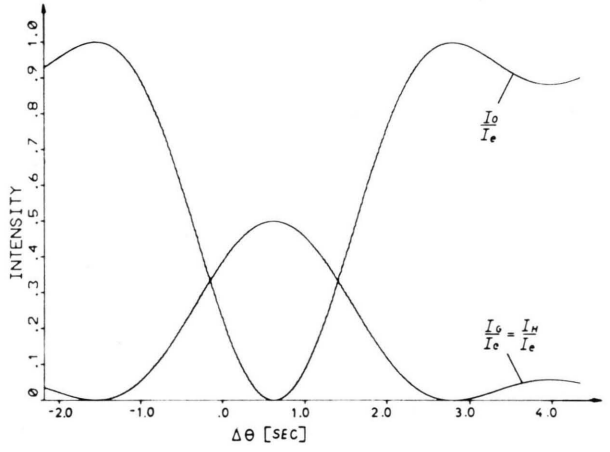

(b)

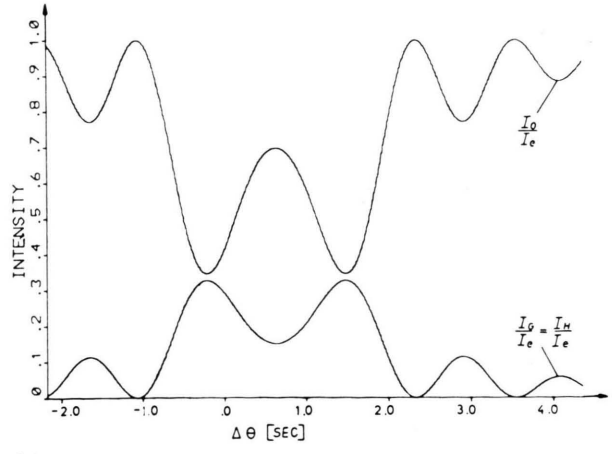

(c)

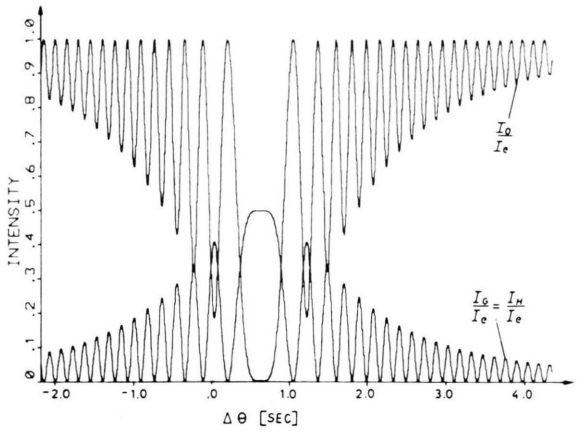

(d)

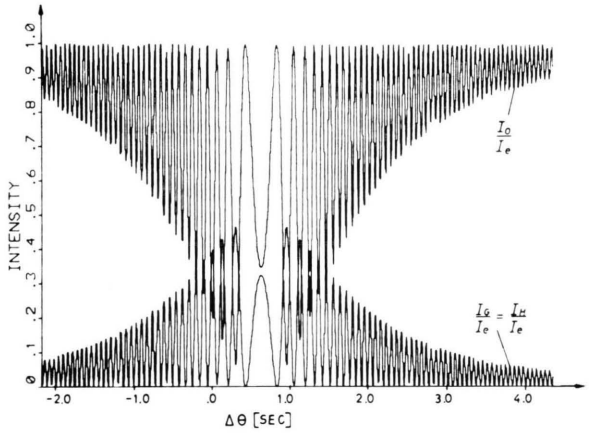

(e)

Fig. 1. Dispersions branches (a) and reflection curves at different thickness (b—e) in the symmetrical treatment ($\alpha = 0$, $\boldsymbol{k}^i$ within the plane of symmetry) as functions of $\Delta\theta$, the deviation from the exact Bragg position. (a) Section of the dispersion surface with (220); I, II and III denote the individual branches. (b)—(e) reflection curves for the forward (I_0/I_e) and the diffracted ($I_G/I_e = I_H/I_e$) relative intensities calculated for crystal thicknesses $D = 0.004219$ cm (half pendellösung period) (b), 0.01 cm (c), 0.08 cm (d), and 0.2 cm (e).

If we now insert the expressions of (15) into the ψ-functions (13) for a definite crystal thickness D and determine the intensity ratios

$$I_0/I_e = I_0\,, \quad I_G/I_e = I_H/I_e = I_G$$

for the 0, G and H directions, then

$$\frac{|\psi_0|^2}{|\psi_e|^2} = I_0(D) = 1 + \frac{2X_2X_3}{X_3 - X_2}\,[1 - \cos(AD)]$$

and (16)

$$\frac{|\psi_G|^2}{|\psi_e|^2} = I_G(D) = 2\left(\frac{X_2X_3}{X_3 - X_2}\right)^2 [1 - \cos(AD)]\,,$$

where

$$A = k(\varepsilon_{0,2} - \varepsilon_{0,3})/\cos\gamma_0$$
$$= kV_0(C_{0,2} - C_{0,3})/\cos\gamma_0\,.$$

From (16) follows that for $D=0$ $I_0 = I_e$ and for any other $D \neq 0$ the relation

$$I_0(D) + I_G(D) + I_H(D) = I_e$$

holds.

The reflection curves of I_0/I_e, I_G/I_e and I_H/I_e in Fig. 1 represent the intensities behind a perfect crystal slab for a given crystal thickness D and $\Delta\theta$, the deviation of $\boldsymbol{k}^i$ from the exact Bragg angle. The angular range of $\boldsymbol{k}^i$ was extended from $-2.2''$ to $4.2''$ in all calculations.

Comparing the dispersion surface of the (111, $\bar{1}\bar{1}$1/220) NTBC with that one of the (111, $\bar{1}$11/200) NTBC (Fig. 1 in [14]) one notices that the individual sheets are different because we have the peculiar case of two intersection branches in the former case. In the point of intersection no determination of the excited amplitudes in respect to the branches is possible; the same holds for the calculation of the strength of the wavefields and intensities emerging into individual directions. On the premises of continuity of the dispersion branches they were calculated to be smooth curves without any step in their shapes. The dispersion sheets themselves are asymmetric in respect to $\Delta\theta = 0$; the individual centers of the branches I and II (the crossing of the asymptotes of I and II) are shifted by $\Delta\theta = 0.65''$. In Figs. 1(b) to (e) reflection curves for different crystal thicknesses are plotted to demonstrate the oscillation frequency as a function of the crystal thickness. Fig. 1 b shows the intensities for the forward (I_0/I_e) beam and both Bragg diffracted beams ($I_G/I_e = I_H/I_e$). At the crystal thickness $D =$ 0.004219 cm apparently I_0/I_e becomes zero at the angle $0.65''$ whereas $I_G/I_e = 0.5$. This thickness equals the half pendellösung period Δ_0 which can be derived from (16).

The intensities of the Bragg diffracted beams are equal, which is obvious because of symmetry arguments for this case. The maximum oscillations occur as well at the angle $0.65''$, independent of the particular crystal thickness. There the intensities vary between 0.0 and 1.0 in the 0 beam (I_0/I_e) and 0.0 and 0.5 in the Bragg diffracted beams ($I_G/I_e = I_H/I_e$) for different thicknesses D. The same result was shown for the (111, $\bar{1}$10/200) NTBC, with the difference that there the oscillations were symmetrical about the exact Bragg angle. The shift of the center of maximum oscillation for all three beams can be explained by the shift of the individual center of symmetry mentioned above.

In the same manner the composition of the ψ functions must be different for the calculation of the intensities. If we compare the formulae for the intensities of the (111, $\bar{1}$11/200) NTBC ((8) in [14]) with those given by (16) in this paper we find additional contributions by the amplitude ratios X_j for the forward and Bragg diffracted intensities. This results in a different Pendellösung period which can be written for this case as

$$\Delta_0 = \frac{2\pi\cos\gamma_0}{\lambda(\varepsilon_{0,2} - \varepsilon_{0,3})} = \frac{\pi\cos\gamma_0}{\lambda b_c N C_{2,3}}$$
$$\text{(substituting } (\varepsilon_{0,2} - \varepsilon_{0,3}) = V_0 C_{2,3})\,.$$

For our NTBC in Si with $\lambda = 1.623 \cdot 10^{-8}$ cm ($V_0 = 1.719 \cdot 10^{-6}$; $\gamma_0 = 26.63°$, $N = 4.99 \cdot 10^{22}$; $b_c = 0.415 \cdot 10^{-12}$ cm; $C_{2,3} = 0.990$), we get $\Delta_0 = 84.4$ μm. One easily can derive the Pendellösung period Δ_0 for the two beam case from this formula if one inserts the Bragg angle into γ_0 and

$$\varepsilon_{0,2} - \varepsilon_{0,3} = V(\boldsymbol{G})/E\,.$$

4. Asymmetrical Incidence

In the asymmetrical case the incoming wave vector $\boldsymbol{k}^i$ is moved off the symmetry plane by the angle $\alpha \neq 0$. Thereby the boundary conditions are not changed so we get now three independent equations

$$\sum_j u_j(\mathbf{0}) = u\,; \quad \sum_j X_j u_j(\mathbf{0}) = 0\,;$$
$$\sum_j Y_j u_j(\mathbf{0}) = 0\,. \qquad (17)$$

The determinant of this inhomogeneous system is given by

$$\Delta = X_1(Y_2 - Y_3) + X_2(Y_3 - Y_1) + X_3(Y_1 - Y_2) \tag{18}$$

and we get the amplitudes $u_j(0)$ from the j-dispersion sheet as

$$u_j(0) = \frac{\varepsilon_{jkl} X_k Y_l}{\Delta} u \tag{19}$$

(cp. (8) in [15]).

Now again we consider the ψ functions representing a propagation in the 0, G or H direction, resp., using the same arguments as in the symmetrical calculation. So similar terms of the ψ function containing parts of the 0, G and H direction are combined to a wavefield propagating in the 0, G of H direction. With (19) ψ_0, ψ_G and ψ_H become

$$\psi_0 = \psi_e \frac{1}{\Delta} \sum_j \varepsilon_{jkl} \exp\left\{ i \frac{k^i \varepsilon_{0,j} D}{\cos \gamma_0} \right\} X_k Y_l , \tag{20}$$

$$\psi_G = \psi_e \frac{e^{i\boldsymbol{G}\cdot\boldsymbol{r}}}{\Delta} \sum_j \varepsilon_{jkl} \exp\left\{ i \frac{k^i \varepsilon_{0,j} D}{\cos \gamma_0} \right\} X_j X_k X_l ,$$

$$\psi_H = \psi_e \frac{e^{i\boldsymbol{H}\cdot\boldsymbol{r}}}{\Delta} \sum_j \varepsilon_{jkl} \exp\left\{ i \frac{k^i \varepsilon_{0,j} D}{\cos \gamma_0} \right\} X_j X_k X_l ,$$

(D means the thickness of the crystal slab).

For the evaluation of the intensity behind a perfect crystal slab of a definite thickness we calculate the product $\psi\psi^*$ and get for the forward direction

$$\begin{aligned} I_0(D)/I_e = {} & |u_1(0)|^2 + |u_2(0)|^2 + |u_3(0)|^2 \\ & + u_1(0)\, u_2^*(0) \exp[iA'(\varepsilon_{0,1} - \varepsilon_{0,2})] \\ & + u_1(0)\, u_3^*(0) \exp[iA'(\varepsilon_{0,1} - \varepsilon_{0,3})] \\ & + u_1^*(0)\, u_2(0) \exp[-iA'(\varepsilon_{0,1} - \varepsilon_{0,2})] \\ & + u_1^*(0)\, u_3(0) \exp[-iA'(\varepsilon_{0,1} - \varepsilon_{0,3})] \\ & + u_2(0)\, u_3^*(0) \exp[iA'(\varepsilon_{0,2} - \varepsilon_{0,3})] \\ & + u_2^*(0)\, u_3(0) \exp[-iA'(\varepsilon_{0,2} - \varepsilon_{0,3})]. \end{aligned} \tag{21}$$

Using the fact that $V(G) = V(-G) = V^*(G) = V^*(-G)$, (21) reduces to

$$\begin{aligned} I_0(D)/I_e = {} & |u_1(0)|^2 + |u_2(0)|^2 + |u_3(0)|^2 \\ & + 2\{u_1(0)\, u_2(0) \cos[A'(\varepsilon_{0,1} - \varepsilon_{0,2})] \\ & + u_1(0)\, u_3(0) \cos[A'(\varepsilon_{0,1} - \varepsilon_{0,3})] \\ & + u_2(0)\, u_3(0) \cos[A'(\varepsilon_{0,2} - \varepsilon_{0,3})]\}. \end{aligned} \tag{22}$$

A similar treatment holds for the G and H intensities.

Defining a tensor τ as

$$\tau_{kl} x_k x_l := x_k x_l + x_k^* x_l \tag{23}$$

and setting $u_j(0) = u_j$ ($j = 1, 2, 3$), we are able to write (21) in a more general form if $A_1 = k/\cos\gamma_0$:

$$\begin{aligned} I_0(D)/I_e = {} & \tfrac{1}{2} \sum_{k,l} \tau_{kl} u_k u_l + \tfrac{1}{2} \sum_{k,l} \tau_{k,l} u_k u_l \\ & \cdot \cos(A_1 D(\varepsilon_{0,k} - \varepsilon_{0,l})] \end{aligned} \tag{24}$$

or

$$\begin{aligned} I_0(D)/I_e = {} & \tfrac{1}{2} \sum_{k,l} \tau_{kl} u_k u_l \\ & \cdot \{1 + \cos[A_1 D(\varepsilon_{0,k} - \varepsilon_{0,l})]\}, \end{aligned}$$

and

$$\begin{aligned} I_G(D)/I_e = {} & \tfrac{1}{2} \sum_{k,l} \tau_{kl} X_k u_k Y_l u_1 \\ & \cdot \{1 + \cos A_1 D(\varepsilon_{0,k} - \varepsilon_{0,l})]\}, \\ I_H(D)/I_e = {} & \tfrac{1}{2} \sum_{k,l} \tau_{kl} Y_k u_k Y_l u_l \\ & \cdot \{1 + \cos[A_1 D(\varepsilon_{0,k} - \varepsilon_{0,l})]\}. \end{aligned} \tag{25}$$

The difference $(\varepsilon_{0,k} - \varepsilon_{0,l})$ can be expressed by the function $f(\varepsilon_{0,k} - \varepsilon_{0,l})$ where f only depends on the difference of the individual excitation errors. The Pendellösung period for this general case may be expressed in the very similar form

$$\Delta = \frac{\pi \cos\gamma_0}{\lambda b_c N f(\varepsilon_{0,i} - \varepsilon_{0,j})},$$

derived from (25), but now excitation errors in connection with the corresponding amplitudes must be inserted. As is shown in Figs. 2 and 3 the "pendelung" developes to a very complicated cooperation due to the presence of all three interfering wavefields in the crystal. For the calculation of the particular intensities the individual excitation errors were determined from (6) and (7). Again $\boldsymbol{k}^i$ was moved through the same angular range of $\pm 6.4''$. The deviation of $\boldsymbol{k}^i$ from the symmetry plane is given by the angle α which can be derived from (8). α defines the angle between $\boldsymbol{k}^i$ of the exact Bragg position and $\boldsymbol{k}^{i'}$ having the same z-component (i.e. [001] component) as $\boldsymbol{k}^i$ but different x- (i.e. [110]) and y- (i.e. [1$\bar{1}$0]) components. In Fig. 2 the dispersion branches I, II, and III are plotted for $\alpha = 2.9''$ and in Fig. 3 for $\alpha = 18.9''$ (Figs. 2 and 3).

The dispersion surfaces in Fig. 2a and Fig. 3a are sections parallel to the (110) netplane. The first striking difference to Fig. 1a are the different shapes of branch I and II. In Fig. 1a they were intersecting each other, but already in a distance of less than $3''$

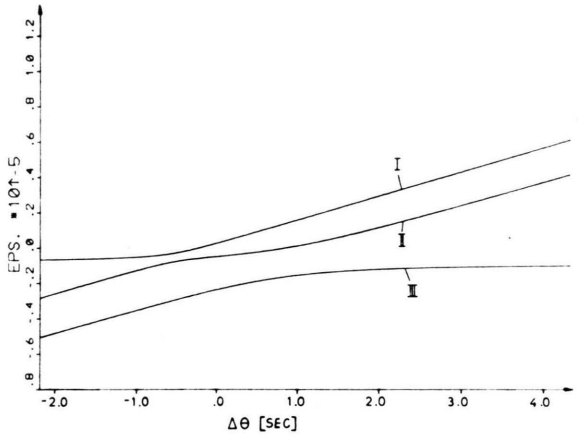

(a)

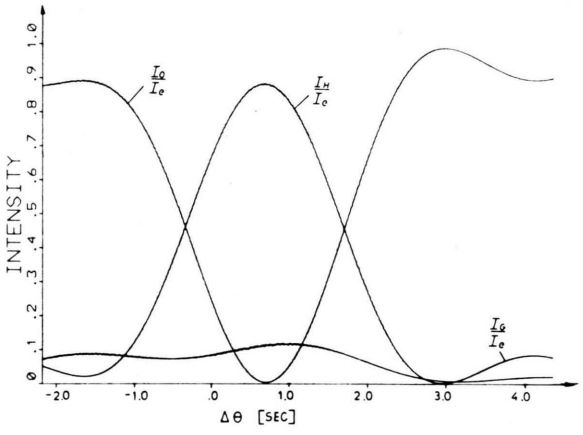

(b)

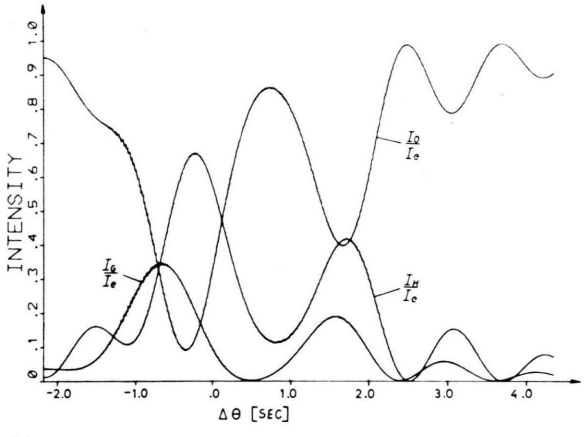

(c)

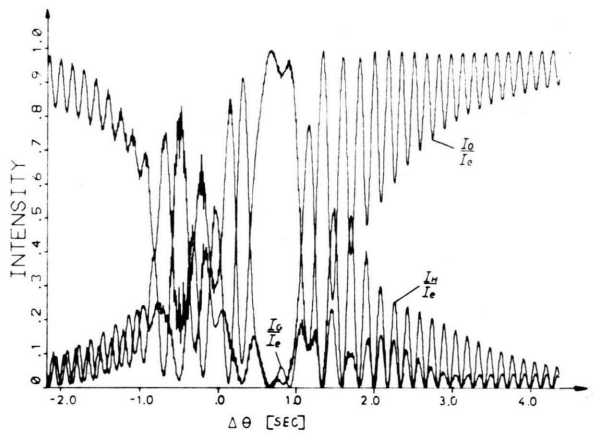

(d)

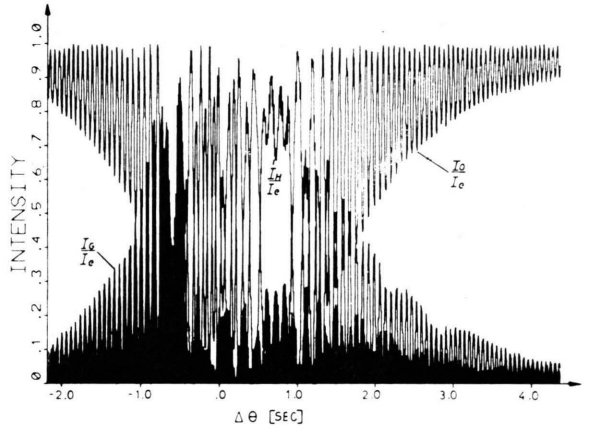

(e)

Fig. 2. Same conditions as in Fig. 1, but asymmetrical treatment with $\alpha = 2.8''$.

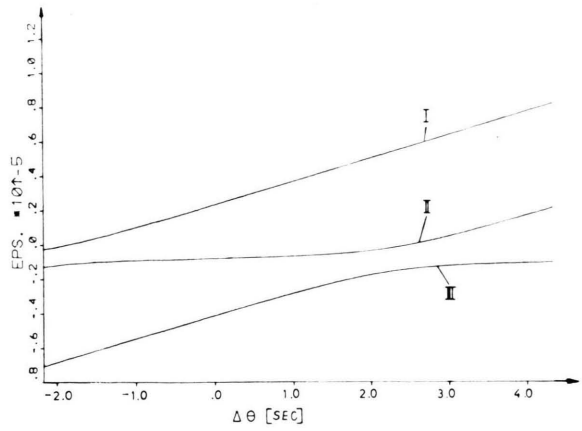

(a)

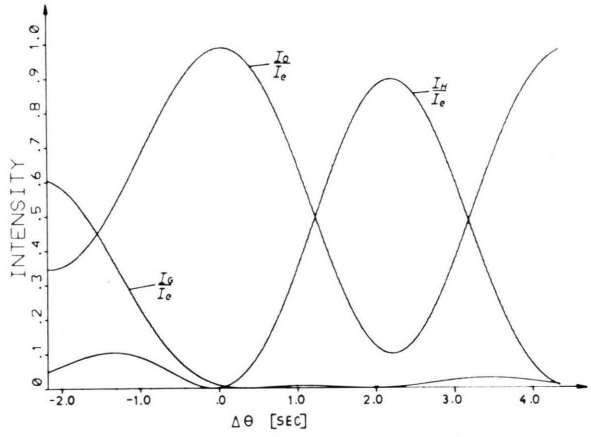

(b)

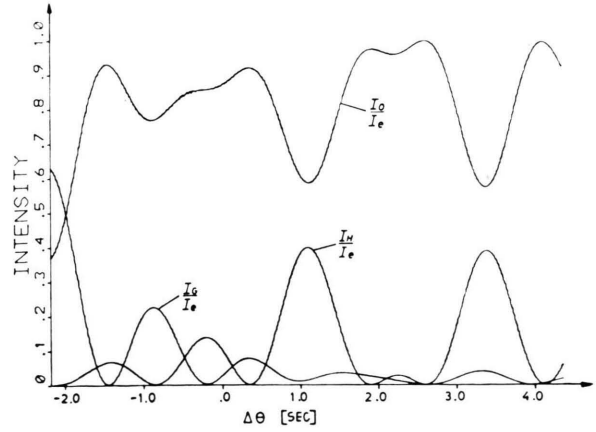

(c)

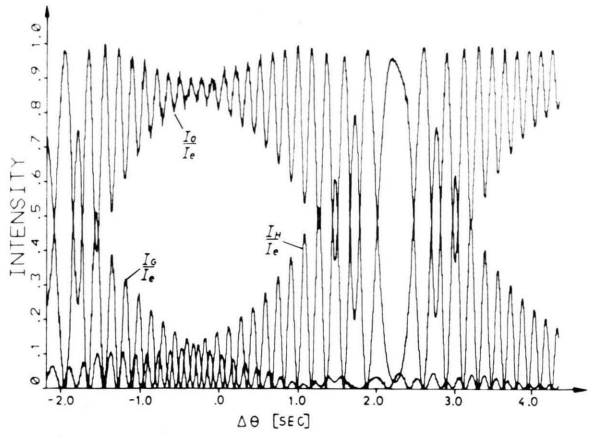

d)

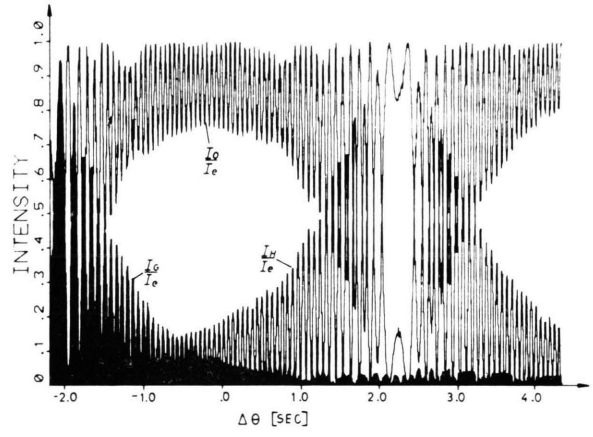

(e)

Fig. 3. Same conditions as in Fig. 2 but $\alpha = 18.9''$.

from the plane of symmetry both are well separated from each other. So the curvatures of sheet I and sheet II must be very strong in this region which can be better seen by the values of the corresponding excitation errors ε at this angle:

From

$$\varepsilon_{01} = -0.2996 \cdot 10^{-5} \text{ and } \varepsilon_{02} = -0.6766 \cdot 10^{-6},$$

valid in the symmetrical case, ε_{01} changes in the asymmetrical case to

$$\varepsilon_{01} = -0.6693 \cdot 10^{-6} \text{ and } \varepsilon_{02} = -0.2883 \cdot 10^{-5},$$

valid for $\alpha = 2.9''$, and to

$$\varepsilon_{01} = -0.2506 \cdot 10^{-6} \text{ and } \varepsilon_{02} = -0.1279 \cdot 10^{-5},$$

valid for $\alpha = 18.9''$, resp. The reflection curves behave similarly sensible. Another difference between the (111, $\bar{1}\bar{1}$1/220) NTBC and the (111, $\bar{1}$11/200) NTBC is the peculiar shape of the reflection curves of the 0, G and H waves especially for small values of α. If the wave vector $\boldsymbol{k}^i$ is further moved out of the (220) plane, the two NTBC's behave more and more similar by (compare Fig. 2 and Fig. 3 in [15]). The crystal thicknesses used in Figs. 2 and 3 are the same as in Fig. 1 (and Figs. in [15]). For the first reflection curve ($D = 0.004219$ cm $= 1/2\Lambda_0$ for the slab) the intensity of the 0 beam seems to be unchanged (besides some asymmetry in the shape of the curve), but the H diffracted beam contains almost the entire intensity of appr. 90% for the angle $\theta = 0.65''$, whereas the intensity of G diffracted beam remains below 10% over an angular range of more than 6''. If we compare the same situation for $\alpha = 18.9''$ then the maximum of the H diffracted beam moves to the left side up to higher angles due to the increased asymmetric incidence of $\boldsymbol{k}^i$. If we increase the crystal thickness D, the intensity oscillations move closer together and are hardly distinguishable. Moving $\boldsymbol{k}^i$ further off the (220) plane the shape of the particular reflection curve is quite the same as in the (111, $\bar{1}$11/200) NTBC. Again the forward beam is oscillating around the Bragg angle, both diffracted beams move off this position at an angle close to $\pm 2''$.

5. Conclusions

The neutron three beam case (NTBC) (111, $\bar{1}\bar{1}$1/220), calculated in this paper, can in two ways be compared to other cases: a) to related X-ray three beam cases, b) to the (seemingly similar) NTBC (111, $\bar{1}$11/200).

a) In NTBC's absorption plays a negligible role in most materials, contrary to TBC's with X-rays; so the conditions for an "enhanced Borrmann effect" are not realized, but on the other hand, due to the simultaneous presence of wave fields from all sheets of the dispersion surface, pronounced Pendellösung effects are to be expected. A simple formula for the Pendellösung period Λ_0, valid for the above mentioned NTBC at symmetrical incidence could be derived which turned out to be very similar to the related formula in a neutron two beam case. The shape of the dispersion surface of this NTBC, intensity ratios of wavefields and other features were only partially comparable to the related X-ray TBC.

b) The NTBC (111, $\bar{1}$11/200), and also the related X-ray TBC have a dispersion surface with a center of symmetry (in the Lorentz point), whereas in the now discussed case the dispersion surface is very asymmetric with respect to the exact three beam point; moreover the wave vectors exhibit a stronger dependence on small deviations of $\boldsymbol{k}_i$ from the exact Bragg direction (all this is also true in the comparable X-ray TBC).

The presence of all excited wavefields throughout the lattice and the strong three dimensional dependence of the wave vector in the crystal now give rise to possible applications of NTBC's in neutron physics: As we have seen, the coherent coupling of the wave fields yields a sensible probe for the investigation of their propagation and their interactions with e.g. weakly deformed lattices because the particular reflection curves react with strong change of their shapes. So the detection of three dimensional strain fields and even of point defects should be possible; other fields of application of NTBC's are (super) small angle scattering as well as high resolution diffraction by the use of a pair of crystals ([20], [21]).

Deviations from the exact Bragg angle can also occur by the change of the neutrons energy. Two beam diffraction experiments with magnetic fields exhibited neutron-energy changes of 10^{-8} eV [22]; in the case of NTBC an even higher resolution is to be expected. The interaction of neutrons with magnetic materials is correlated to spin related dynamics such as polarization, Larmor precession and magnetic refraction. The study of these phenomena in NTBC opens new aspects which must give rise to new experiments and methods.

Acknowledgements

The author has enjoyed many helpful discussions with Prof. G. Hildebrandt and wish to thank him for his help and encouragement for this work. Further he is indebted to B. Rückert and Chr. Zimmermann for their helpful assistence and grand support for this article.

[1] M. Renninger, Z. Kristallogr. A **97**, 107 (1937); M. Renninger, Naturwiss. **25**, 43 (1937).
[2] G. Borrmann and W. Hartwig, Z. Kristallogr. **121**, 401 (1965).
[3] G. Hildebrandt, phys. stat. sol. **24**, 245 (1967).
[4] W. Uebach, G. Hildebrandt, Z. Kristallogr. **129**, 1 (1969). W. Uebach, Z. Naturforsch. **289**, 7 (1973). G. Hildebrandt and W. Scherz, Acta Cryst. **A34**, S232 (1978).
[5] W. Scherz and G. Hildebrandt, Z. Naturforsch. **36a**, 921 (1981).
[6] M. Umeno and G. Hildebrandt, phys. stat. sol. a **31**, 583 (1975).
[7] G. Hildebrandt, Krist. Tech. **13**, 1095 (1978).
[8] P. P. Ewald, Ann. Phys. **54**, 519 (1917); P. P. Ewald, Rev. Mod. Phys. **37**, 46 (1965).
[9] J. W. Knowles, Acta Cryst. **9**, 61 (1965).
[10] D. Sippel, K. Kleinstück, and G. E. R. Schulze, phys. stat. sol. **2**, 104 (1962). D. Sippel, K. Kleinstück, and G. E. R. Schulze, Phys. Lett. **14**, 174 (1965).
[11] F. Eichhorn and D. Sippel, Wiss. Z. TU-Dresden **20**, 423 (1971).
[12] C. G. Shull, A. Zeilinger, G. L. Squires, M. A. Horn, D. K. Atwood, and J. Arthur, Phys. Rev. Lett. **44**, 26 (1980).
[13] C. G. Shull, Phys. Rev. Lett. **21**, 1585 (1968).
[14] W. Treimer, Phys. Lett. **68A**, 2 (1978).
[15] W. Treimer, Z. Naturforsch. **33a**, 1432 (1978).
[16] W. Mashall and S. W. Lovesey, Theory of Thermal Neutron Scattering. Oxford Press, London 1971.
[17] E. Fermi, Ric. Sci. **7**, 2 (1936).
[18] M. v. Laue, Röntgenstrahlinterferenzen, Akad. Verl. Ges., Graz 1960.
[19] W. H. Zachariasen, Theory of X-Ray Diffraction in Crystal, Dover Publ.
[20] U. Bonse and R. Teworte, J. Appl. Cryst. **13**, 410 (1980).
[21] U. Bonse and R. Teworte, J. Phys. E; Sci. Instrum. **15**, 187 (1982).
[22] A. Zeilinger and C. G. Shull, Phys. Rev. B **19**, 3957 (1979).